Available online at www.sciencedirect.com
ScienceDirect
Journal of Photochemistry and Photobiology A: Chemistry 195 (2008) 81–88
Journal of Photochemistry and Photobiology A:Chemistry
www.elsevier.com/locate/jphotochem

Enhancement effect of TiO_2 dispersion over alumina on the photocatalytic removal of NO_x admixtures from O_2–N_2 flow

Boris N. Shelimov [a,*], Nikolai N. Tolkachev [a], Olga P. Tkachenko [a], Galina N. Baeva [a], Konstantin V. Klementiev [b], Alexander Yu. Stakheev [a], Vladimir B. Kazansky [a]

[a] *N.D. Zelinsky Institute of Organic Chemistry, Russian Academy of Sciences, Leninskii pr. 47, 119991 Moscow, Russia*
[b] *ALBA Synchrotron, CELLS, Campus UAB, 08193 Bellaterra, Barcelona, Spain*

Received 23 May 2007; received in revised form 14 September 2007; accepted 18 September 2007
Available online 25 September 2007

Abstract

The efficiencies of bulk TiO_2 Degussa P-25 and TiO_2 dispersed over alumina support in the photocatalytic removal of NO_x ($NO + NO_2$) admixtures from flowing NO–O_2–N_2 mixture modeling polluted air are compared. The TiO_2/Al_2O_3 samples with different Ti contents prepared by the sol–gel method are characterized by BET, XAFS and diffuse-reflectance UV–vis spectroscopy. At a TiO_2 content above approximately 20 wt%, a thermally stable anatase phase is formed in TiO_2/Al_2O_3 in which the Ti ions are six-coordinated. As the TiO_2 content diminishes from ~20 to 1 wt%, the titanium coordination number gradually decreases, and the TiO_2 phase is no longer detected. Most likely, isolated Ti ions in different coordinations are predominant in such samples. It is found that, upon UV irradiation, NO oxidation to NO_2 in flowing NO–O_2–N_2 readily occurs over bulk TiO_2 and TiO_2/Al_2O_3 at TiO_2 loadings higher than ~20 wt%. No photoreaction is observed on Al_2O_3 without TiO_2 and on TiO_2/Al_2O_3 at TiO_2 loadings below ~10 wt%. Correlating these results with the XAFS and UV–vis data, it is concluded that the presence of a TiO_2 phase on the alumina surface is a prerequisite for the photocatalytic activity in the NO oxidation. The outlet concentrations of NO and NO_2 as a function of irradiation time are measured, and absorption capacities of the photocatalysts to NO_x are quantitatively assessed. The performance of TiO_2/Al_2O_3 is superior than that of bulk TiO_2, because much larger amounts of NO_2 formed by the photoreaction can be strongly trapped by the support. The highest adsorption capacity per unit catalyst weight is found for 50% TiO_2/Al_2O_3. The NO_x adsorption capacity of bulk TiO_2 is found to increase upon humidification of the reaction gas mixture.

Keywords: Air pollution; NO_x removal; Photocatalysis; UV irradiation; XAFS; UV–vis spectroscopy

1. Introduction

Currently photocatalytic methods of indoor air purification from organic and inorganic pollutants are intensively being developed. In most cases titanium dioxide is used as a photocatalyst, because it is highly active in degrading many organic and inorganic air pollutants, is biologically and chemically inert and is of low cost [1–3]. Upon irradiation of TiO_2 by UV light with photon energies exceeding the band gap (>3.0 eV for rutile or >3.2 eV for anatase), a complete oxidation (mineralization) of various organic substances adsorbed on its surface by air oxygen readily occurs. Titanium dioxide is also applied for air purification from nitrogen oxides (mainly from NO) [4–7]. Upon UV irradiation of TiO_2 in air or in O_2–N_2 mixtures polluted with NO, nitrogen dioxide is produced which partly evolves into the gas phase and partly remains adsorbed on the TiO_2 surface. In addition, IR spectroscopy reveals surface nitrate-like species containing a NO_3^- fragment [8–10]. Because the active sites of TiO_2 are blocked by adsorbed NO_2 and nitrates, the photocatalyst gradually loses its photoactivity, and the NO_x concentration ($NO_x = NO + NO_2$) at the outlet of the photocatalytic reactor tends to approach the initial inlet NO concentration. The life time of the photocatalyst depends on many factors such as, for instance, initial NO concentration, amount of TiO_2 in the photocatalytic reactor, flow rate, humidity of the polluted air, etc. Photocatalytic activity of TiO_2 can be completely restored by

* Corresponding author.
E-mail address: bns@ioc.ac.ru (B.N. Shelimov).

1010-6030/$ – see front matter © 2007 Elsevier B.V. All rights reserved.
doi:10.1016/j.jphotochem.2007.09.009

heating the catalyst in an air or inert-gas flow at 400–500 °C or by washing the catalyst with water which results in the removal of adsorbed nitrate- and nitrite-like species blocking the active sites on the surface [4].

Thus, it becomes evident that, because of gradual photocatalyst poisoning by the reaction products, it is not possible to accomplish a long-term continuous photocatalytic conversion of NO in a flow photoreactor system without intermediate catalyst regeneration. However, the efficiency of the photocatalyst, i.e., the total amount of NO_x absorbed on the photocatalyst until full inhibition of its activity can be considerably increased by applying mechanical mixtures of TiO_2 with adsorbents of a high adsorption capacity, for example, TiO_2 mixtures with zeolites A and Y [10] or with active carbon [11–13]. In these systems, the major part of NO_2 produced on TiO_2 is captured by the adsorbents, while the active sites of TiO_2 remain unoccupied. Even a more efficient way to increase the TiO_2 performance in the photocatalytic deNO_x was employed by Ichiura et al. [14]: they used thin composite sheets prepared from a mixture of pulp slurry and suspension of TiO_2 and basic oxides (CaO, MgO) or $CaCO_3$. Nitrogen dioxide and HNO_3 formed in the photoreaction are neutralized by the oxides or carbonate, and the amount of the NO_x removed per unit weight of TiO_2 considerably increases.

Another approach that enables one to substantially increase the lifetime of TiO_2 photocatalysts was used in [11–13,15]. The feasibility of applying photocatalytic technology for simultaneous removal of NO and aromatic compounds (benzene, toluene, ethylbenzene and *o*-xylene) which are most abundant in the indoor air was investigated. At initial NO and aromatics concentrations of 0.2 and 0.03–0.04 ppm, respectively, no deactivation of TiO_2 is found to occur even after prolonged UV irradiation (for around 6 h). The steady-state NO_x concentration is as low as ~0.025 ppm, and the aromatics concentration decreases to 0.005–0.007 ppm [15].

As shown in a series of publications by Tanaka, Teramura et al. [16–18], selective catalytic photoreduction of NO by ammonia is a very efficient way for NO removal from indoor air. The photoreduction can be accomplished upon UV irradiation of TiO_2 in a flow of NO (1000 ppm), NH_3 (1000 ppm), 2–10% O_2, and Ar (balance) at room temperature. A 83% NO conversion at a 96% selectivity to N_2 can be reached in this system. It is worth noting that, when ammonia is present in the flow, NO oxidation by oxygen is replaced by NO reduction with NH_3 according to the following equation: $4NO + 4NH_3 + O_2 \rightarrow 4N_2 + 6H_2O$. This reaction is well known and widely used in practice for the catalytic purification of exhaust gases produced by stationary power plants using V_2O_5–WO_3/TiO_2, MoO_3–WO_3/TiO_2 and other catalysts [19].

The present study was aimed at elucidating the factors that may affect activity, selectivity and stability of Ti-containing bulk and supported photocatalysts for NO_x removal from NO–O_2–N_2 mixtures taken as a model of polluted air and at improving the lifetime and performance of the photocatalysts. High-surface area alumina widely used as a catalyst support was chosen for the TiO_2 dispersion. This material is known to exhibit high adsorption capacity towards NO_2—the major product of the photoreaction [20–23].

2. Experimental

2.1. Preparation of Ti-containing samples

Commercial TiO_2 Degussa P-25 ($S = 55\ m^2\ g^{-1}$) and TiO_2/Al_2O_3 samples prepared by the sol–gel method (hereafter denoted as $TiAl_{sg}$) with TiO_2 loadings of 96, 50, 23, 10 and 1 wt% were used.

The $TiAl_{sg}$ samples were prepared from sols of Al and Ti hydroxides. The Al sol was obtained by dissolving $Al(C_3H_7O)_3$ (98%, Aldrich) in hot distilled water at 90–95 °C ($H_2O/Al = 100$) followed by adding 1.4 M HNO_3 ($HNO_3/Al = 0.07$) upon vigorous stirring for 1 h at 95 °C. The Al concentration in the resulting sol was 0.015 g/mL.

The titanium hydroxide sol was obtained from a 6% solution of $Ti(C_3H_7O)_4$ (97%, Aldrich) in isopropanol. A mixture of isopropanol, 1.4 M HNO_3 and water was added dropwise under stirring to the isopropanol solution for 2 h ($H_2O/Ti = 4$, $HNO_3/Ti = 0.05$, $C_3H_7OH/Ti = 70$). The Ti concentration in the sol was 0.008 g/mL.

The Al and Ti sols thus prepared were mixed in various proportions depending on the TiO_2 content. The sol mixture was stirred for 0.5 h, and then the liquid phase was removed at 60 °C using a rotor evaporator. The resulting solids were calcined in air flow at 500 °C for 2 h (the rate of temperature rise was 0.2 °C min^{-1} at 20–120 °C and 0.5 °C min^{-1} at 120–500 °C).

For reference, a Ti-ZSM-5 sample was prepared by the CVD method. Zeolite HZSM-5 ($Si/Al = 15$) was exposed to $TiCl_4$ vapor in flowing He at 400–500 °C followed by water vapor hydrolysis of the Ti-species at 300 °C. Another Ti-ZSM-5 sample was prepared using twice the same CVD procedure. The Ti content varied from 1.8 wt% (1 CVD) to 5 wt% (2 CVD).

2.2. Characterization of Ti-containing catalysts

Specific surface area (SSA) of the $TiAl_{sg}$ samples was determined by the BET method by air adsorption at 77 K as described in [24]. The SSA values were 19, 275, 336 and 290 $m^2\ g^{-1}$ for $TiAl_{sg}$ samples with TiO_2 loadings 96, 50, 23 and 10 wt%, respectively.

XAFS measurements were carried out at HASYLAB (DESY in Hamburg, Germany) on the beamline E4 (Ti K-edge, 4966 eV) using a double-crystal Si(1 1 1) monochromator, which was detuned to 50% of maximum intensity to exclude higher harmonics in the X-ray beam. For XAFS analysis, 7–25 mg samples were mixed with polyethylene, pressed into self-supported pellets (13 mm in diameter) and mounted to the vacuum chamber. The spectra were recorded in the transmission mode at 80 K. The spectra were measured several times in order to check reproducibility. Reference spectra were recorded using standard reference compounds: TiO_2 (rutile and anatase) and Ti-foil. Analysis of the XAFS (XANES and EXAFS) spectra was performed with the software VIPER for Windows [25]. The fitting was done in *k*- and *r*-spaces. The shell radius, coordination number, Debye–Waller factor and adjustable 'muffin-tin zero' were determined as fitting parameters.

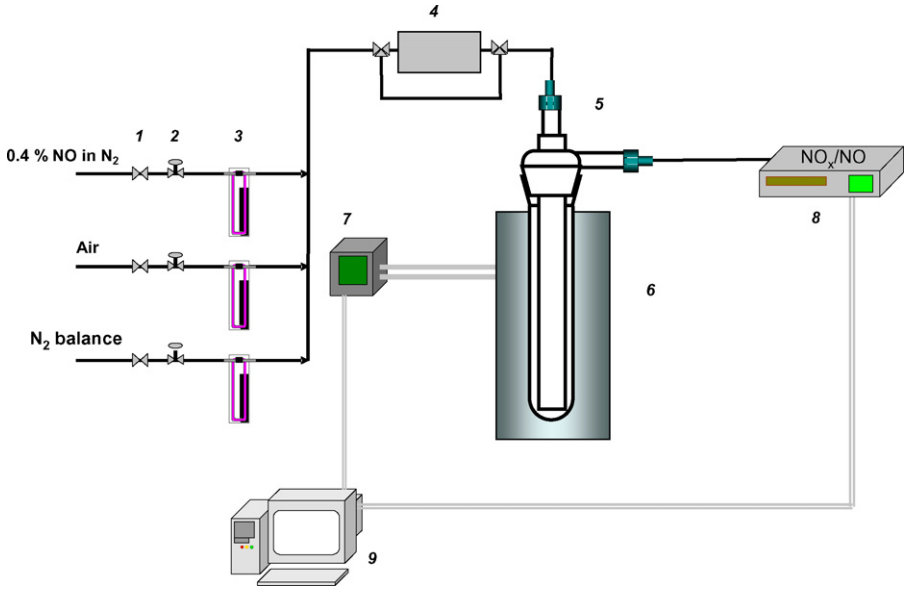

Fig. 1. Experimental setup—1: valves; 2: needle valves; 3: flow meters; 4: water vapor saturator; 5: quartz photoreactor; 6: furnace; 7: temperature controller; 8: NO_x analyzer; 9: PC.

Diffuse reflectance UV–vis spectra (200–900 nm region) were recorded on a Specord M40 spectrophotometer supplied with an integration sphere. A pellet made of a pressed MgO powder was used as reference.

2.3. Photocatalytic experiments

A tubular quartz photoreactor ($d = 30$ mm, $h = 250$ mm) was used in these experiments. A thin layer of the Ti-catalyst was deposited on the inner walls of the reactor from a suspension of finely ground powder in distilled water. After deposition, the reactor was dried at 120 °C overnight. The catalyst weight in the reactor was about 0.2 g.

The photocatalytic NO oxidation was performed at atmospheric pressure and ambient temperature using the setup shown in Fig. 1. The 0.4% NO in N_2, air and N_2 streams (Linde Gas Rus) were mixed using needle valves to obtain the desired NO and O_2 concentrations and to adjust gas flow rate (440 mL/min). In some experiments, the gaseous mixture was humidified by passing through a water saturator at 20 °C.

The catalyst in the photoreactor was first activated in flowing dried air at 500 °C for 1 h. Then the furnace was removed, the reactor was allowed to cool down to ambient temperature, and a mixture of 45–50 ppm NO, 7 vol.% O_2 and N_2 (balance) modeling polluted air was flowed until equal NO concentrations at the inlet and outlet of the photoreactor were achieved. Thereafter the catalyst in the photoreactor was irradiated from both sides with two compact 26 W black lights (Camelion, LH26-30). The light intensity was measured with a Photex UVA radiometer and a set of color filters in the range of 320–390 nm. The light intensity distribution was as follows: 3.5% at 420–390 nm; 19.5% at 390–370 nm; 47% at 370–350 nm; 25% at 350–320 nm; 5% at 320–290 nm.

NO and NO_2 concentrations were measured with a chemiluminescent NO–NO_x gas analyzer (Eco Physics, model CD70S) or with an IR gas analyzer (Tement Instruments, модель Gasmet^{TM} Dx-4000n) at a 5-s interval.

The temperature ramp during temperature-programmed desorption (TPD) experiments was 10 °C/min.

3. Results and discussion

3.1. Characterization of Ti-samples

3.1.1. XANES and EXAFS

Fig. 2 depicts the XANES spectra of $TiAl_{sg}$, Ti-ZSM-5 (CVD) and two TiO_2 modifications (anatase and rutile) which were used as reference samples.

The XANES spectra of 96 and 50% $TiAl_{sg}$ in the pre-edge region are very similar to that of bulk anatase. This suggests formation of an anatase phase on the alumina surface which is stable up to 500 °C. For the 10 wt% TiO_2 loading, the spectrum in the pre-edge region displays a single peak characteristic of isolated

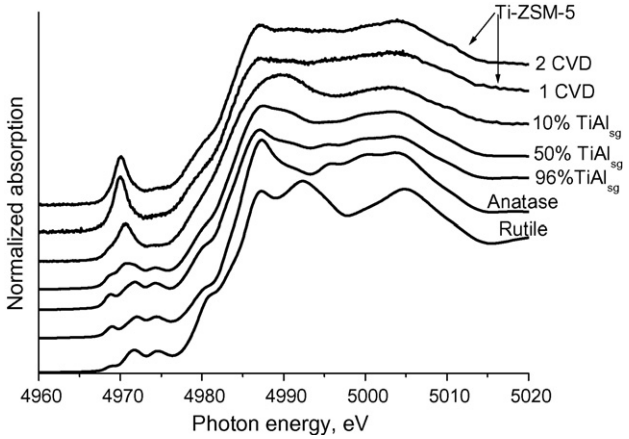

Fig. 2. Normalized XANES spectra of $TiAl_{sg}$, Ti-ZSM-5 (CVD) and bulk TiO_2.

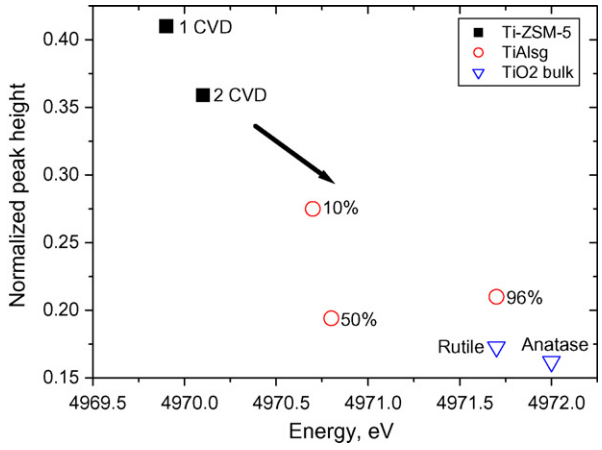

Fig. 3. Normalized pre-edge height vs. energy position for Ti K-pre-edge features.

Ti^{4+} ions or small Ti^{4+}-containing clusters. Similar spectra were obtained for the Ti-ZSM-5 samples (1 and 2 CVD).

A more precise analysis of the coordination state of Ti was performed using the method of Farges et al. [26]. With both the pre-edge peak position and normalized height it is possible to asses the Ti coordination number (CN). The results are summarized in Fig. 3 in which the arrow depicts a direction of increasing CN of Ti ions. Like in bulk TiO_2, the CN in 96% $TiAl_{sg}$ is close to 6. At lower TiO_2 content (50% $TiAl_{sg}$), Ti is penta- and hexacoordinated. The fraction of pentacoordinated Ti atoms increases at lower loading (10%). A mixture of tetra- and pentacoordinated Ti atoms is found in Ti-ZSM-5. The second CVD treatment results only in a minor increase of the average coordination number.

Additional information about the local structure of Ti atoms was obtained from EXAFS data (Fig. 4). The calculated Ti–O distances and CN are presented in Table 1. EXAFS spectra of 96 and 50% $TiAl_{sg}$ are very similar to those of rutile and anatase. The calculated CNs are 6 and 5, respectively in agreement with the XANES data analysis. EXAFS spectra of 10% $TiAl_{sg}$ and both Ti-ZSM-5 (1 and 2 CVD) differ markedly from the reference substances. They show the absence of a TiO_2 phase and the presence of mononuclear $Ti^{4+}O_x$ species with a distorted octahedral oxygen coordinated sphere. It should be noted that the Ti CNs of Ti^{4+} derived from EXAFS data are more reliable than those obtained from XANES. Therefore, small discrepancies between the CNs determined by these two techniques appears to be quite reasonable.

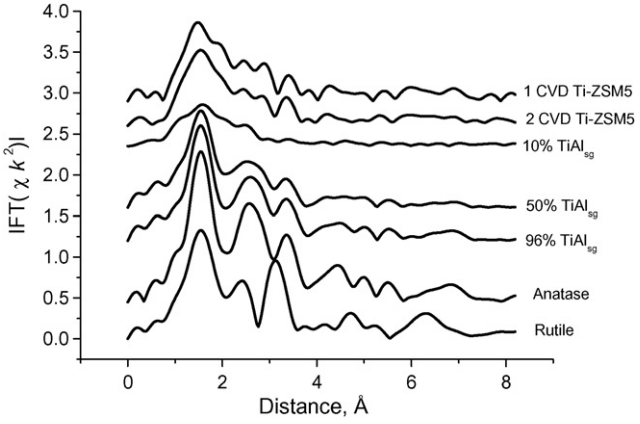

Fig. 4. EXAFS spectra of $TiAl_{sg}$, Ti-ZSM-5 (CVD) and bulk TiO_2.

Table 1
EXAFS data analysis of TiO_2-based samples

Sample	Ti–O distance (Å)	Coordination number	Debye–Waller factor
Rutile	1.952 ± 0.07 2.031 ± 0.27	3.7 ± 0.4 1.8 ± 0.1	0.005 ± 0.001 0.006 ± 0.001
96% $TiAl_{sg}$	1.954 ± 0.08 2.033 ± 0.29	3.9 ± 0.4 1.7 ± 0.5	0.005 ± 0.001 0.010 ± 0.002
50% $TiAl_{sg}$	1.951 ± 0.09 2.032 ± 0.33	3.8 ± 0.4 0.9 ± 0.4	0.006 ± 0.001 0.004 ± 0.005

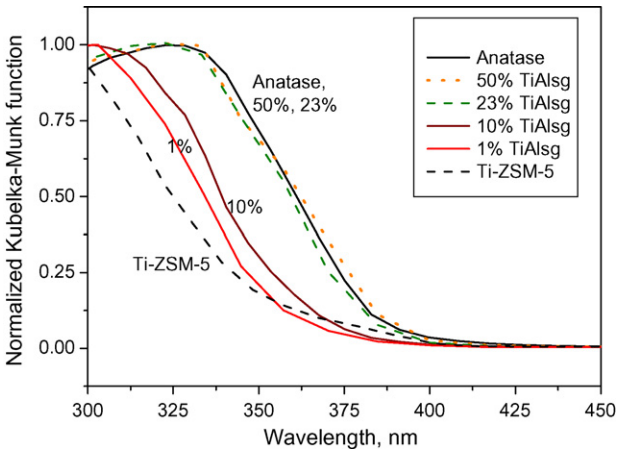

Fig. 5. Diffuse reflectance UV–vis spectra of anatase, $TiAl_{sg}$ and Ti-ZSM-5.

3.1.2. UV–vis spectra

The spectra of 23, 50 and 96 wt% $TiAl_{sg}$ (Fig. 5)[1] are very similar to that of bulk anatase in accord with the above XAFS data suggesting the formation of an anatase phase in these samples. For $TiAl_{sg}$ with TiO_2 loadings of 10 wt% or less and for the CVD Ti-ZSM-5 samples, a marked blue shift of the long-wave absorption edge is observed. The blue shift for $TiAl_{sg}$ depends on the Ti content and is 0.22 eV for 10% $TiAl_{sg}$ and 0.27 eV for 1% $TiAl_{sg}$. The largest shift (0.32 eV) is found for Ti-ZSM-5.

The blue shift of the absorption edge can be associated with various effects. First, it may be linked to the formation of TiO_2 nanoparticles of 1–5 nm in diameter in $TiAl_{sg}$ at low Ti loadings, i.e., to the quantum size effect of semiconductor particles [2]. In this case, the TiO_2 nanoparticles on alumina surface retain the crystal lattice structure of rutile or anatase, and the blue shift results from an increase in the effective band gap of the

[1] Spectrum of 96% TiAlsg is not shown in Fig. 5.

semiconductor because of the small particle size. The alternative explanation suggests the formation of isolated low-coordinated Ti ions in the $TiAl_{sg}$ structure or the localization of these ions in the ZSM-5 channels. In this case, the UV absorption band arises from the charge transfer from O^{2-} to a neighbor Ti^{4+} ion, and the energy of this transition depends on the Ti ion coordination. This hypothesis agrees well with the XAFS data: no TiO_2 phase was found by this technique in $TiAl_{sg}$ at low Ti loadings and in Ti-ZSM-5, while the CN of Ti ions tends to decrease.

The results obtained by XAFS and UV–vis spectroscopy can be summarized as follows.

1. Local environment and coordination number of Ti^{4+} ions incorporated into alumina and ZSM-5 are governed both by the titanium content and the nature of the support.
2. At high TiO_2 contents (>20 wt%), an anatase phase with Ti CN = 6 is formed in $TiAl_{sg}$ which is stable up to 500 °C. As the TiO_2 content diminishes from ~20 to 1 wt%, the CN gradually decreases, and the blue shift of the UV-light absorption edge increases. In such samples, the fraction of isolated Ti ions with different coordination environments appears to be predominant.

   This conclusion agrees with the earlier XRD and XPS results [27]: no TiO_2 phase is found in $TiAl_{sg}$ at TiO_2 loadings below 15 wt%, and the Ti^{4+} ions are uniformly distributed inside alumina particles.
3. In Ti-ZSM-5 obtained by CVD, the CN of Ti ions is close to 4, and these ions are highly dispersed. Isolated Ti ions or small clusters are suggested to be predominant in these samples.

3.2. Photocatalytic NO removal

It is found in blank tests that, in the absence of UV irradiation, NO concentration in the gaseous NO–O_2–N_2 mixture flowing over TiO_2 and $TiAl_{sg}$ does not change, at least, for 2 h and no NO_2 is detected at the outlet. Upon UV irradiation of bulk TiO_2, 23 and 50% $TiAl_{sg}$ under the flow, NO is readily oxidized to NO_2. On the contrary, when alumina without TiO_2 or $TiAl_{sg}$ with TiO_2 loadings of 10% or less are UV irradiated, the outlet NO concentration does not change and gaseous NO_2 is not detected. Correlating these findings with the XAFS and UV–vis characterization of $TiAl_{sg}$ (see Section 3.1), we can conclude that the necessary prerequisite for the catalytic activity is the presence of a TiO_2 phase in the photocatalyst in which spatial separation of the photoinduced electrons and holes and their migration to the semiconductor surface can occur.

It is worth noting that, upon UV irradiation of bulk or supported TiO_2 in pure NO or in its mixtures with inert gases (He, N_2), NO is reduced to N_2 and N_2O, the latter being a predominant product [28–31]. Contrary to that, the reduction of NO is fully suppressed if some oxygen is present, and no N_2O is found among the reaction products (Fig. 6).

For bulk TiO_2, and 23 and 50% $TiAl_{sg}$, the outlet concentrations of NO, NO_2 and NO_x ($NO_x = NO + NO_2$) as a fuction of irradiation time have been measured (Figs. 6–8). The following common features are typical for these photocatalysts. Just

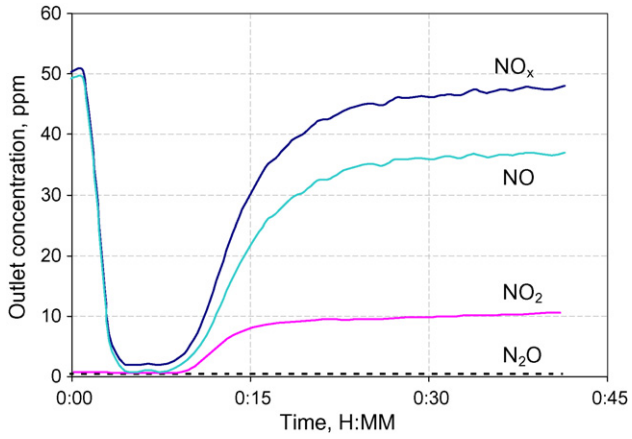

Fig. 6. Time dependence of outlet NO, NO_2, NO_x and N_2O concentrations upon UV irradiation of bulk TiO_2.

after the start of irradiation, the outlet NO_x concentration rapidly drops to a minimum value (NO_x(min)), remains at this minimum level for a certain time (retention time, t(ret)), and then slowly grows approaching a steady state in which NO_x(ss) is nearly equal to the inlet NO concentration. For bulk TiO_2, the outlet NO_x concentration nearly reaches the inlet NO concentration within approximately 30 min after the onset of irradiation, i.e., no purification from oxides of nitrogen actually occurs at the

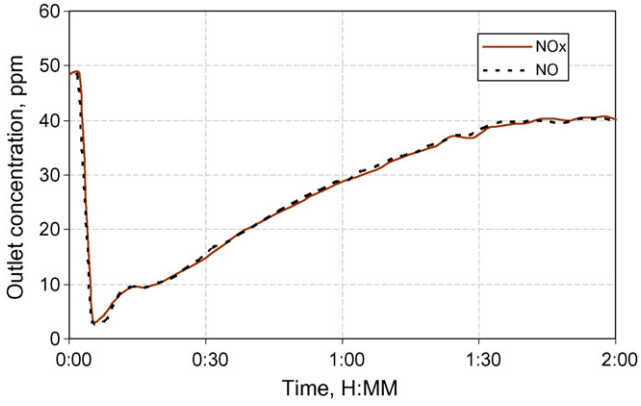

Fig. 7. Time dependence of outlet NO and NO_x concentrations upon UV irradiation of 23% $TiAl_{sg}$.

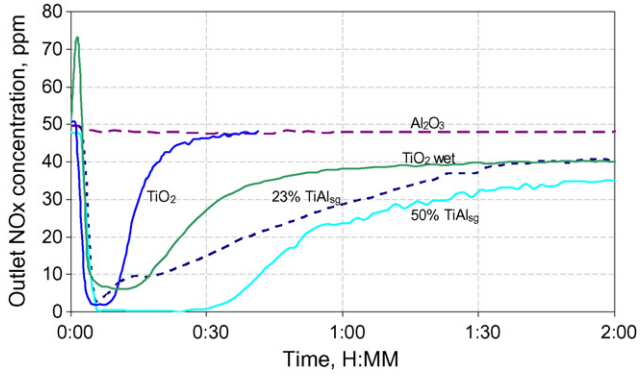

Fig. 8. Time dependence of outlet NO_x concentration upon UV irradiation of the photocatalysts.

Table 2
Photoadsorption capacity to NO_x of the TiO_2-based photocatalysts

Photocatalyst	Inlet NO concentration (ppm)	Specific photoadsorption capacity	
		μmole NO_x g(Cat)$^{-1}$	mole NO_x (mole TiO_2)$^{-1}$ × 10^2
TiO_2 Degussa P-25	55	60	0.48
	35 (H_2O)[a]	104	0.83
50% $TiAl_{sg}$	48	320	5.12
23% $TiAl_{sg}$	48	180	7.18
	60	205	8.19
	145	131	5.22
	46 (H_2O)[a]	61	2.45
10% $TiAl_{sg}$	50	No activity	

[a] Humidified gaseous mixture.

steady state (Fig. 6). Similar results have earlier been reported in [4]. Supported 23 and 50% $TiAl_{sg}$ demonstrate much better stability: even after 2 h of irradiation, the outlet NO_x concentration is by 20–30% less than the inlet NO concentration, i.e. the photocatalytic deNO_x although incomplete still occurs (Fig. 8). The initial photoactivity of all the catalysts is fully restored by heating in flowing dry air at 450–500 °C.

It should be noted that the outlet NO concentrations for bulk TiO_2 and 50% $TiAl_{sg}$ at the steady state are markedly lower than the inlet NO concentration (Fig. 6 illustrates this for bulk TiO_2). The outlet NO_2/NO ratio under the steady state depends on TiO_2/Al_2O_3 ratio in the photocatalyst. The NO_2/NO ratio is 0.25–0.27 for bulk TiO_2 (Fig. 6), whereas the NO_2 fraction considerably decreases for 50% $TiAl_{sg}$, and the NO_2/NO ratio drops to 0.09–0.11. For 23% $TiAl_{sg}$, all NO_2 produced by the photoreaction remains adsorbed (Fig. 7). Hence, the NO_2/NO ratio for a specific photocatalyst is controlled by the rate of NO oxidation to NO_2 and by the rate of NO_2 adsorption on the catalyst.

The efficiencies of the photocatalysts in the removal of nitrogen oxides from the O_2–N_2 flow have been quantitatively assessed by calculating the total amount of NO_x adsorbed by the photocatalysts for 2 h of UV irradiation by integrating the kinetic curves of Fig. 8. The specific capacities per 1 g of the catalysts or per 1 mole of TiO_2 in the catalysts are given in Table 2. The specific adsorption capacities of 50 and 23% $TiAl_{sg}$ per 1 g of the catalyst exceed that of bulk TiO_2 by a factor of 5.3 and 3.0, respectively at approximately equal initial NO content of 48–55 ppm. The difference in the adsorption capacity per 1 mole of TiO_2 is even higher. Thus, the performance of the photocatalysts with TiO_2 dispersed on alumina with highly developed surface is considerably superior than that of bulk TiO_2, because much larger amounts of NO_2 formed by the photoreaction can be strongly trapped by the support.

It is worth noting that the supported catalysts far exceed bulk TiO_2 in the retention time (t_{ret}). For example, t_{ret} is about 30 min for 50% $TiAl_{sg}$ at NO_x(min) concentration close to zero, while t_{ret} is around 4–5 min for bulk TiO_2 at NO_x(min) concentration of 2–3 ppm (Fig. 8).

Humidification of the initial gaseous mixture favors the removal of oxides of nitrogen on bulk TiO_2: specific adsorption capacity to NO_x is enhanced by a factor of 1.5–2 (Table 2) and t_{ret} increases to ~15 min at a simultaneous insignificant increase of the minimum NO_x concentration to 7 ppm (Fig. 8). During the first several minutes of irradiation, a momentary release of NO_2 into the gas phase is observed which is apparently due to photodesorption of the NO_2 accumulated on TiO_2 surface during preliminary dark exposure to the initial gas mixture owing to partial NO oxidation. After approximately 2 h of irradiation, the outlet NO_x concentration reaches ~80% of the inlet NO concentration. However, the analysis of the outlet gas shows that the NO_2/NO ratio equals one, i.e., considerably greater than that for the dry gaseous mixture. No promoting effect of gaseous mixture humidification is found for 23% $TiAl_{sg}$ (Table 2).

At the present time, the mechanism of NO photooxidation by oxygen on TiO_2 is not known in detail. It is often suggested the key role of OH radicals and anion-radicals O_2^- formed upon the capture of photogenerated holes and electrons by surface hydroxyls and oxygen molecules [4,32]:

$$TiO_2 \overset{h\nu}{\rightleftharpoons} h^+ + e^- \quad (1)$$

$$OH^- + h^+ \rightleftharpoons {}^\bullet OH \quad (2)$$

$$O_2 + e^- \rightleftharpoons O_2^- \quad (3)$$

where h^+ and e^- are hole and electron centers, respectively. Reactions (2) and (3) suggest spatial separation and migration of the photoinduced electrons and holes to the TiO_2 surface.

The NO oxidation proceeds by the following sequence of reactions:

$$NO + {}^\bullet OH \rightleftharpoons HNO_2 \quad (4)$$

$$HNO_2 + {}^\bullet OH \rightleftharpoons NO_2 + H_2O \quad (5)$$

$$NO_2 + {}^\bullet OH \rightleftharpoons HNO_3 \quad (6)$$

$$NO + O_2^- \rightleftharpoons NO_3^- \quad (7)$$

The increase in the adsorption capacity of TiO_2 upon humidification of the gaseous mixture may be linked to the following effects. First, the production of $^\bullet OH$ radicals may increase by the following reaction:

$$H_2O + h^+ \rightleftharpoons {}^\bullet OH + H^+ \quad (8)$$

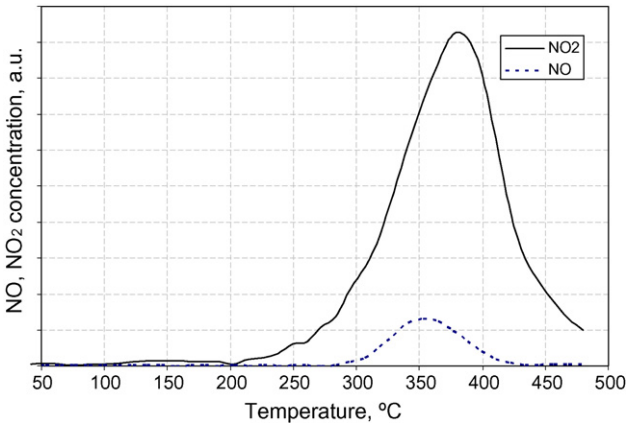

Fig. 9. TPD spectrum of bulk TiO_2 after the photoreaction.

As a result, the rate of NO oxidation by reactions (4)–(6) can grow. Second, water can wash out, at least partly, NO_2 and HNO_3 from the surface thus liberating the active sites necessary for photocatalysis.

3.3. TPD after UV irradiation

After the steady state in the photoreaction had been achieved, UV lamps were turned off, the catalysts were purged with dry nitrogen at room temperature, and then TPD measurements were carried out. In the case of bulk TiO_2, NO_2 is the major desorption product (T_{max} = 375 °C), while the fraction of NO desorbed (T_{max} = 355 °C) is only 10% (Fig. 9).

It appears that both peaks arise from the decomposition of nitrate and nitrite species accumulated on the TiO_2 surface in the course of photooxidation. On the contrary, for 23% $TiAl_{sg}$, the low-temperature NO desorption peak (T_{max} = 150 °C) dominates in the TPD spectrum, and the NO_2 fraction (T_{max} = 160–180 °C) is much less significant (Fig. 10). Most likely, these peaks are linked to the desorption of NO and NO_2 from the alumina surface: according to [23], oxides of nitrogen desorb from pure Al_2O_3 in this temperature interval. The relatively small high-temperature desorption peaks at 400–430 °C in Fig. 10 presumably arise from the decomposition of N-containing species on the titania surface.

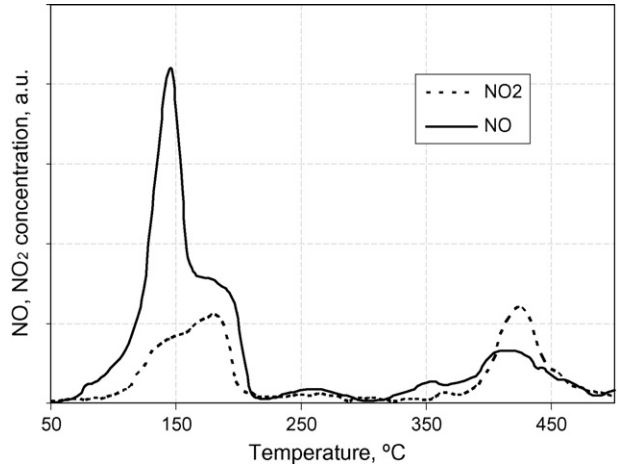

Fig. 10. TPD spectrum of 23% $TiAl_{sg}$ after the photoreaction.

4. Conclusion

The performance of Ti-based catalysts for the photocatalytic removal of NO_x from a gaseous O_2–N_2 mixture polluted by NO can be largely improved by dispersion of TiO_2 over a high surface-area alumina. The specific adsorption capacities to NO_x of 50 and 23% $TiAl_{sg}$ per catalyst unit weight exceed that of bulk TiO_2 by a factor of 5.3 and 3.0, respectively, at approximately equal initial NO contents in the gaseous mixture. The necessary prerequisite for the catalytic activity is the presence of a TiO_2 phase in $TiAl_{sg}$ which is evidenced by XAFS and UV–vis spectroscopy at TiO_2 contents higher than ~20 wt%. The TiO_2 semiconductor phase provides fast migration of the photoinduced electrons and holes to the surface to produce $^{\bullet}OH$ radicals and anion-radicals O_2^- from hydroxyls, adsorbed H_2O and O_2 molecules which apparently play a key role in the NO photoxidation to NO_2, HNO_3 and nitrate species.

By contrast, upon UV irradiation of the $TiAl_{sg}$ samples with low Ti contents, in which the fraction of isolated low-coordinated Ti^{4+} ions is high, localized $(Ti^{3+}–O^-)^*$ pairs are predominantly created by the photoinduced charge transfer from lattice oxygen to the Ti^{4+} ions. It appears that this transition state is inefficient in the $^{\bullet}OH$ and O_2^- production likely because of fast deactivation and recombination.

A pronounced promoting effect of humidification of the reaction-mixture on the adsorption capacity to NO_x found for bulk TiO_2 is also worth noting. Most likely, the effect is linked to faster $^{\bullet}OH$ radical production from adsorbed water as well as to the liberation of the blocked active sites by washing strongly adsorbed reaction products.

Acknowledgements

This work was supported by INTAS under grant 03-51-6088 and by the Russian Foundation for Basic Research under grant 05-03-32490. The authors thank HASYLAB (DESY, Germany) for providing X-ray beam time (project I-20060226 EC).

References

[1] A. Mills, S. Le Hunte, J. Photochem. Photobiol. A: Chem. 108 (1997) 1.
[2] A.L. Linsebigler, G. Lu, J.T. Yates Jr., Chem. Rev. 95 (1995) 735.
[3] A. Fujishima, X. Zhang, C.R. Chimie 9 (2006) 750.
[4] S. Devahasdin, C. Fan Jr., K. Li, D.H. Chen, J. Photochem. Photobiol. A: Chem. 156 (2003) 161.
[5] M. Inagaki, T. Inai, T. Yoshkawa, B. Tryba, Appl. Catal. B: Environ. 51 (2004) 247.
[6] S. Matsuda, H. Hatano, Powder Technol. 151 (2005) 61.
[7] F.B. Li, X.Z. Li, C.H. Ao, M.F. Hou, S.C. Lee, Appl. Catal. B: Environ. 54 (2004) 275.
[8] A.V. Alekseev, V.N. Filimonov, Russ. J. Phys. Chem. 58 (1984) 2023.
[9] J.C.S. Wu, Yu-T. Cheng, J. Catal. 237 (2006) 393.
[10] K. Hashimoto, K. Wasada, M. Osaki, E. Shono, K. Adachi, N. Toukai, H. Kominami, Y. Kera, Appl. Catal. B: Environ. 30 (2001) 429.
[11] C.H. Ao, S.C. Lee, Appl. Catal. B: Environ. 44 (2003) 191.
[12] C.H. Ao, S.C. Lee, J. Photochem. Photobiol. A: Chem. 165 (2004) 131.

[13] C.H. Ao, S.C. Lee, Chem. Eng. Sci. 60 (2005) 103.
[14] H. Ichiura, T. Kitaoka, H. Tanaka, Chemosphere 51 (2003) 855.
[15] C.H. Ao, S.C. Lee, C.L. Mak, L.Y. Chan, Appl. Catal. B: Environ. 42 (2003) 119.
[16] T. Tanaka, K. Teramura, K. Arakaki, T. Funabiki, Chem. Commun. (2002) 2742.
[17] K. Teramura, T. Tanaka, T. Funabiki, Langmuir 19 (2003) 1209.
[18] K. Teramura, T. Tanaka, S. Yamazoe, K. Arakaki, T. Funabiki, Appl. Catal. B: Environ. 53 (2004) 29.
[19] H. Bosch, F. Janssen, Catal. Today 2 (1988) 369.
[20] V.H. Grassian, J. Phys. Chem. A 106 (2002) 860.
[21] C. Börensen, U. Kirchner, V. Scheer, R. Vogt, R. Zellner, J. Phys. Chem. A 104 (2000) 5036.
[22] G.M. Underwood, T.M. Miller, V.H. Grassian, J. Phys. Chem. A 103 (1999) 6184.
[23] A.A. Lisachenko, A.O. Klimovskii, R.V. Mikhailov, B.N. Shelimov, M. Che, Appl. Catal. B: Environ. 67 (2006) 127.
[24] A.L. Klyachko-Gurvich, Bull Acad. Sci. USSR, Div Chem. Sci. (1961) 1884.
[25] K.V. Klementiev, VIPER for Windows (Visual Processing in EXAFS Researches), freeware. http://www.desy.de/∼klmn/viper.html.
[26] F. Farges, G.E. Brown, J.J. Rehr, Phys. Rev. B 56 (1997) 1809.
[27] A. Yu Stakheev, G.N. Baeva, N.S. Telegina, I.V. Mishin, T.R. Brueva, G.I. Kapustin, L.M. Kustov, Stud. Surf. Sci. Catal. 143 (2002) 509.
[28] N.W. Cant, J.R. Cole, J. Catal. 134 (1992) 317.
[29] T.H. Lim, S.M. Jeong, S.D. Kim, J. Gyenis, J. Photochem. Photobiol. A: Chem. 134 (2000) 209.
[30] J. Zhang, T. Ayusawa, M. Minagawa, K. Kinugawa, H. Yamashita, M. Matsuoka, M. Anpo, J. Catal. 198 (2001) 1.
[31] N. Bowering, G.S. Walker, P.G. Harrison, Appl. Catal. B: Environ. 62 (2006) 208.
[32] J.S. Dalton, P.A. Janes, N.G. Jones, J.A. Nicholson, K.R. Hallam, G.C. Allen, Environ. Pollut. 120 (2002) 415.